African Journal of Biotechnology Vol. 8 (5), pp. 745-750, 6 March, 2009
Available online at http://www.academicjournals.org/AJB
ISSN 1684–5315 © 2009 Academic Journals

Full Length Research Paper

Deformation of skull bone as intracranial pressure changing

Xianfang Yue* and Li Wang

School of Mechanical Engineering, University of Science and Technology Beijing, Beijing 100083, China.

Accepted 31 March, 2008

Raised intracranial pressure (ICP), a serious and often fatal condition, is often not preventable. In the present study, the relationship was determined between cranial deformation and ICP change. To record the deformation of skull bone, strain foil was placed on the exterior surface of parietal skull. Prior to construction of finite-element model (FEM), using the rats, an *in vivo* study was undertaken. Three anesthetized adult rats were subjected to baseline recording followed by either experimental raising ICP. By using the 'Ansys' finite element processor, a three-dimensional FEM of a hollow sphere was constructed for human skull. The model was used to calculate the deformation of human skull with the intracranial pressure changing. The skull is a layered sphere constructed in a specially designed form with a Tabula externa, Tabula interna, and a porous Diploe sandwiched in between. The stress and strain deformations were well-proportional on the exterior surface of human skull. The deformation scope of human skull was theoretically from 1.0 to 3.4 με with the changing ICP from 1.5 to 5.0 kPa. The cranium could move and human skull - dura mater system was deformed as the ICP fluctuates.

Key words: Deformation, skull bone, intracranial pressure, finite-element model, rat.

INTRODUCTION

Dr. Sutherland (1939) firstly perceived a subtle palpable movement within the bones of cranium. Dr. Upledger (Retzlaff et al., 1973) discovered that the inherent rhythmmic motion of cranial bones was caused by the fluctuation of cerebrospinal fluid (CSF).

The 'Monro (1823) - Kellie (1824) doctrine' states that an adult cranial compartment is incompressible, and the volume inside the cranium is a fixed volume thus creates a state of volume equilibrium, such that any increase of the volumes of one component (i.e. blood, CSF, or brain tissue) must be compensated by a decrease in the volume of another. If this cannot be achieved then pressure will rise and once the compliance of the intracranial space is exhausted then small changes in volume can lead to potentially lethal increases in intracranial pressure (ICP). The compensatory mechanism for intracranial space occupation obviously has limits. When the amount of CSF and venous blood that can be extruded from the skull has been exhausted, the ICP becomes unstable and waves of pressure develop (Lundberg, 1960). As the process of space occupation continues, the ICP can rise to very high levels and the brain can become displaced from its normal position. The objective of this study was to determine the relationship between cranial deformation and ICP change.

*Corresponding author. E-mail: yuexf@me.ustb.edu.cn. Tel: +86-01-62332743. Fax: +86-10-62329145.

MATERIALS AND METHODS

Prior to construction of the finite-element model (FEM), an *in vivo* study was undertaken using the rats. The deformations of the human skull-dura mater system were measured using strain gauge. Under the same loading conditions, the displacements of skull-dura mater system were calculated using the FEM.

Strain foil was placed on the exterior surface of parietal skull to record the strains of skull bone. ICP variation was recorded simultaneously via strain foils on the skull. Three anesthetized adult rats were subjected to baseline recording followed by either experimental raising ICP induced by middle cerebral artery occlusion (MCAO). MCAO was produced as the model of raising ICP, and a computer continuously recorded the strains of skull bone. ICP variation could be obtained through the automatic processing based on the deformations of skull bone.

For the purpose of our analysis, we adopted a model consisted of a hollow sphere. By using the 'Ansys' finite element processor, an

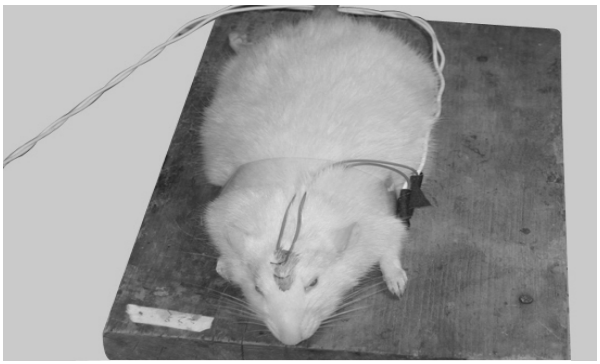

Figure 1. Display effect after pasting strain foils on the rat's head.

initial three-dimensional FEM of a human skull was constructed. The model was used to calculate the deformation of human skull with the ICP changing.

Animal experiments

In the previous analysis, the skull deformation can reflect the ICP change. Some studies monitored ICP in animal models for a prolonged time (Jallo et al., 1997; Kusaka et al., 2004; Miller et al., 1984).

An *in vivo* study was undertaken on three anesthetized adult rats. Three adult rats weighing 320, 400 and 430 g were anesthetized by intraperitoneal injection of alpha-chloralose (60 mg/kg) and urethane (40 mg/kg). First a midline linear skin incision was made on the parietal skull of rats. The area was shaved for about 11 mm^2 and cleansed with alcohol and betadine. After drying, an incision was made and the skin and periosteum was pulled back until the parietal skull was visible. The BX120-2AA strain foil was placed at the measuring point with glue (Figure 1) and pressed with fingers for 2 min. Then the skin and periosteum were put back and the interrupted sutures were operated. The leading-out wires of strain foils were connected with the CM-1J-20 strain gauge. The insulating resistance was kept more than 50 megohm.

Middle cerebral artery occlusion (MCAO) was adopted as the model of raising ICP. MCAO was produced by passing a nylon thread up through the internal carotid artery and piecing a hole on the arterial wall at the middle cerebral artery. The reproduction of the MCAO model used Brint's method (Brint et al., 1988). By either experimental raising ICP induced by MCAO, rats were subjected to baseline recording followed. The rats were allowed to breathe room air spontaneously, and the femoral arterial blood pressure was continuously monitored. In all rats, baseline ICP was recorded for 1 h. During this period, the deformations of skull bone were tested by strain gauge in all rats and a computer continuously recorded the strains of skull bone.

Theoretical analysis

The craniospinal cavity may be considered as a balloon. For the purpose of our analysis, we adopted a model consisted of a hollow sphere. We presented the development and the validation of a 3D finite-element human skull model intended to better understand the deformation mechanism of human skull corresponding to the ICP change. Four different entities were distinguished in the complex anatomy of the cranial cavity: Tabula externa, Tabula interna, and porous Diploe sandwiched in between. Based on the established

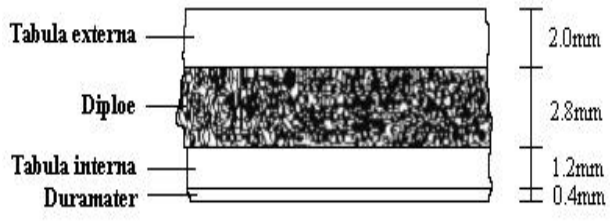

Figure 2. Sketch of layered cranial-cavity sphere. The thin-walled structure of cranial cavity is mainly composed of Tabula externa, Diploe, Tabula interna and dura mater.

knowledge of cranial cavity importantly composed of skull and dura mater (Figure 2), a thin-walled structure was simulated by the composite shell elements of the finite-element software (Piekarshi et al., 1973). The important mechanical characteristic of cancellous bone and dura mater is viscoelasticity (Odgaard, 1997; Noort et al., 1981).

ICP is not a static state, but one that is influenced by several factors. It can rise sharply with coughing and sneezing, up to 50 or 60 mmHg to settle down to normal values in a short time. It also varies according to the activity the person is involved with. For these reasons single measurement of ICP is not a true representation. ICP needs to be measured over a period. The brain appears to be mild injury when ICP variation is about 2.5 kPa, moderate injury when ICP variation is about 3.5 kPa and severe injury when ICP variation is about or more than 5 kPa. Therefore, the following theoretical analysis was carried out within the ICP scope from 1.5 to 5 kPa.

In this work, the finite-element software ANSYS was applied to theoretically analyze the deformation of human skull with the changing ICP. The external diameter of cranial cavity is about 200 mm. The thickness of shell is the mean thickness of calvarias. The average thickness of adult's calvaria is 6.0 mm, that of Tabula externa is 2.0 mm, diploe is 2.8 mm, Tabula interna is 1.2 mm and, dura mater in the parietal position is 0.4 mm.

The combined models made up of the primary elements are usually adopted to describe the viscoelastic performance of actual materials. The creep of linear viscoelastic solid can be simulated by the Kelvin model of three parameters or the generalized Kelvin model.

Viscoelastic model of human skull

Kelvin model of three parameters is shown in Figure 3a. Figure 3b shows the relaxation curves of human skull and Kelvin model of three parameters in the compressive experiment. Figure 3c is the creep curves of human skull and Kelvin model of three parameters. So the theoretical Kelvin model of three parameters could well simulate the mechanical properties of human skull in the tensile experiments. Thus the Kelvin model of three parameters was adopted to describe the viscoelasticity of human skull in this paper.
For the Kelvin model of three parameters, the stress and strain of human skull are shown in equation (1),

$$\begin{cases} \varepsilon = \varepsilon_0 + \varepsilon_1 \\ \sigma = E_1\varepsilon_1 + \eta\dot{\varepsilon_1} \\ \sigma = E_0\varepsilon_0 \end{cases} \quad (1)$$

After the calculation based on the equation (1), the elastic modulus

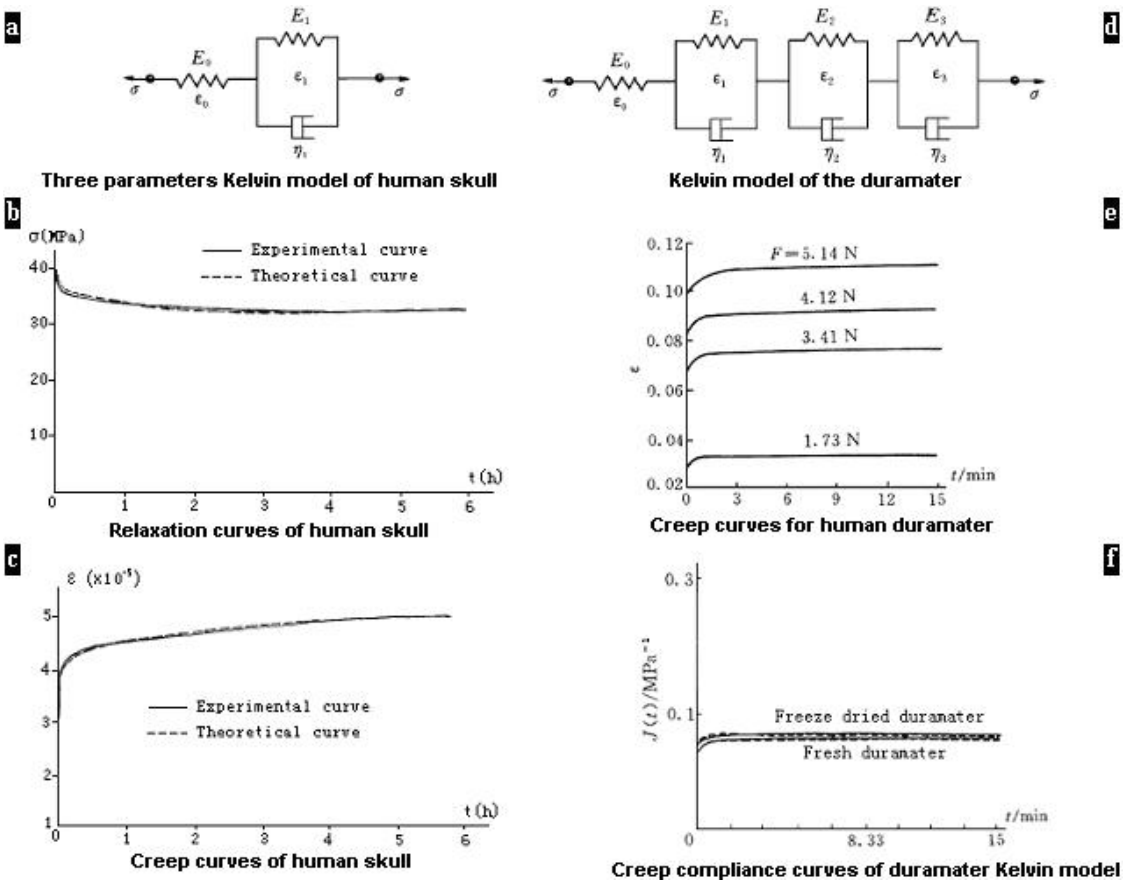

Figure 3. Viscoelastic Kelvin model of human skull and dura mater. **a**. Three-parameters Kelvin model of human skull. **b**. Relaxation train-time curves of the experiment and three-parameters Kelvin theoretical model for human skull. **c**. Creep train-time curves of the experiment and three-parameters Kelvin theoretical model for human skull. **d**. Generalized Kelvin model of the human dura mater. **e**. Creep train-time curves under different actions for fresh human dura mater (L_0 = 23 mm, θ = 37°). **f**. Creep compliance curves of generalized Kelvin model for human dura mater.

of human skull is equation (2),

$$E = \left(\frac{E_0 E_1}{E_0 + E_1}\right) + \left(\frac{E_0^2}{E_0 + E_1}\right) e^{\frac{t}{P_1}} \quad (2)$$

Here, σ = direct stress acted on elastic spring or impact stress acted on viscopot, ε = direct strain of elastic spring; E = elastic modulus of tensile compression; η = viscosity coefficient of viscopot; $\dot{\varepsilon}$ = strain ratio; and

$$P_1 = \frac{\eta}{E_0 + E_1}$$

Viscoelastic model of human dura mater

The generalized Kelvin model is shown in Figure 3d. Figure 3e is the creep experimental curves of human dura mater. Figure 3f is the curves of creep compliance for the generalized Kelvin model. The tendency of creep curve in the experiment was coincident with that of creep compliance for the generalized Kelvin model. Creep is the change law of material deformation with time under the invariable stress, so here σ is constant. For the generalized Kelvin model, the stress-strain relationship is:

$$\varepsilon(t) = J(t)\sigma$$

Thus the tendency of theoretical creep curve is totally the same as that of experimental one for human dura mater. So in this paper, the generalized Kelvin model composed of three Kelvin-unit chains and a spring was adopted to simulate the viscoelasticity of human dura mater in this paper.

For the viscoelastic model of human dura mater composed of the three Kelvin-unit chains and a spring, the stress and strain of human dura mater were shown in equation (3),

$$\begin{cases} \varepsilon = \varepsilon_0 + \varepsilon_1 + \varepsilon_2 + \varepsilon_3 \\ \varepsilon_0 = \dfrac{\sigma}{E_0} \\ \sigma = E_1\varepsilon_1 + \eta_1\dot{\varepsilon_1} = E_2\varepsilon_2 + \eta_2\dot{\varepsilon_2} = E_3\varepsilon_3 + \eta_3\dot{\varepsilon_3} \end{cases} \quad (3)$$

After the calculation based on the equation (3), the creep com-

Table 1. Coefficients for the viscoelastic properties of human skull.

Parameter	Elastic modulus (GPa)		Viscosity (GPa/s	Delay time (s)	
	E_0	E_1	η	τ_γ^*	τ_d^*
Compression	5.69±0.26	42.24±2.09	96840±5400	2022±198	2292±246
Tension	13.64±0.59	51.45±2.54	206100±15360	3180±300	4026±372

Table 2. Creep coefficients for the viscoelastic properties of fresh human duramater.

Parameter	Elastic modulus (MPa)				Delay time (s)		
	E_0	E_1	E_2	E_3	τ_1	τ_2	τ_3
Dura mater	16.67	125.0	150.0	93.75	40	10^4	10^6

pliance of human dura mater is equation (4),

$$J(t)=E_0^{-1}+E(1-e^{-t/\tau_1})+E_2^{-1}(1-e^{-t/\tau_2})+E_3^{-1}(1-e^{-t/\tau_3}) \quad 4$$

Then the elastic modulus of human dura mater is equation (5),

$$E=\left[E_0^{-1}+E_1^{-1}\left(1-e^{-t/\tau_1}\right)+E_2^{-1}\left(1-e^{-t/\tau_2}\right)+E_3^{-1}\left(1-e^{-t/\tau_3}\right)\right]^{-1} \quad 5$$

Here, σ, ε, E, η, $\dot{\varepsilon}$ = Ditto mark; τ_1, τ_2, τ_3 = Lag time, that is $\tau_1=\eta_1/E_1$, $\tau_2=\eta_2/E_2$, $\tau_3=\eta_3/E_3$.

In the finite-element software ANSYS, there are three kinds of models to describe the viscoelasticity of actual materials, in which the Maxwell model is the general designation for the combined Kelvin and Maxwell models. Considering the mechanical properties of human skull and dura mater, the finite-element Maxwell model was adopted to simulate the viscoelasticity of human skull-dura mater system. The viscoelastic parameters of human skull and dura mater are respectively listed in Tables 1 and 2.

Human skull is the viscoelastic material (Charalambopoulos et al., 1998). Considering the viscoelasticity of human skull and dura mater, we used the viscoelastic option of the ANSYS finite-element program to analysis the strains on the exterior surface of human skull as ICP changing. According to the symmetry of 3D model of human skull, the preprocessor of the ANSYS finite-element program was used to construct a 1/8 FEM of human skull and dura mater consisting of 25224 nodes and 24150 three-dimensional 8-node isoparametric solid elements, shown in Figure 4f.

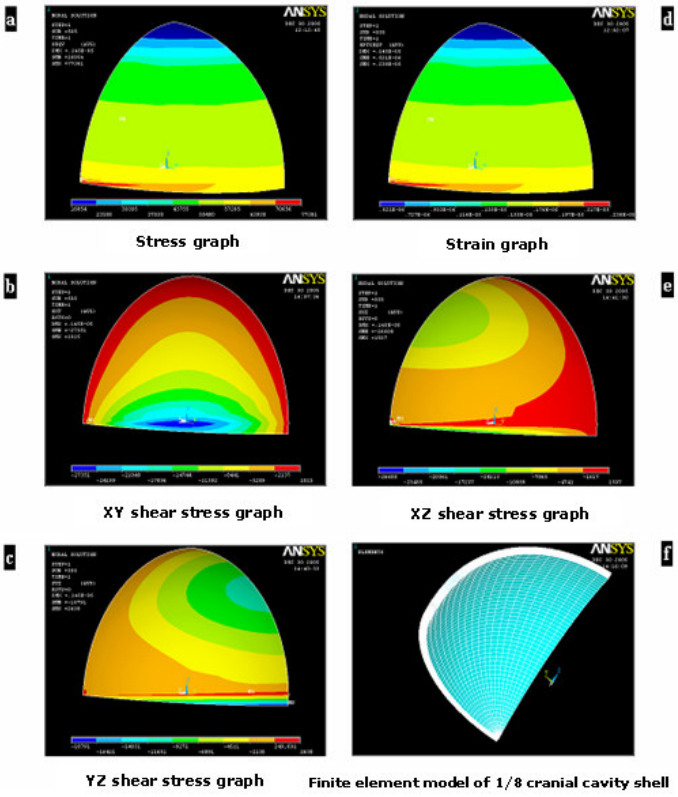

Figure 4. FEA of strains of cranial cavity by considering the viscoelasticity of human skull and dura mater with finite-element software ANSYS when the ICP increment is 2.5 kPa. **a**. Stress graph. **b**. Strain graph. **c**. XY shear stress graph. **d**. XZ shear stress graph. **e**. YZ shear stress graph. **f**. FEM of 1/8 cranial cavity shell.

RESULTS

Figures 4 a to e are the analytic graphs of stress and strain with finite-element software ANSYS when ICP variation is raised up to 2.5 kPa. The stress and strain distributions were well-proportioned on the exterior surface of human skull. Human skulls were deformed with the ICP change. As the ICP changing from 1.5 to 5 kPa, the strains of cranial cavity are shown in Figure 5 with the finite-element software ANSYS. The strains of cranial cavity were coincident with ICP variation.

In three rats in the MACO group, the blood vessels were obstructed within 30 min after passing a nylon

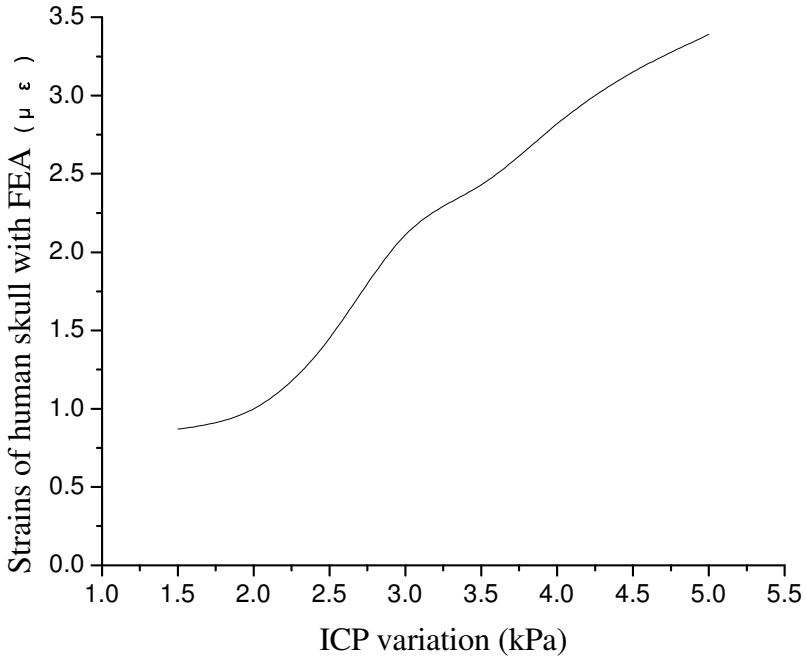

Figure 5. Strain curves of human skulls of the theoretical FEA and simulative experiment with the changing ICP. The deformation strains of mild injury, moderate injury and severe injury are separately 1.6, 2.9 and 4.0 με or so.

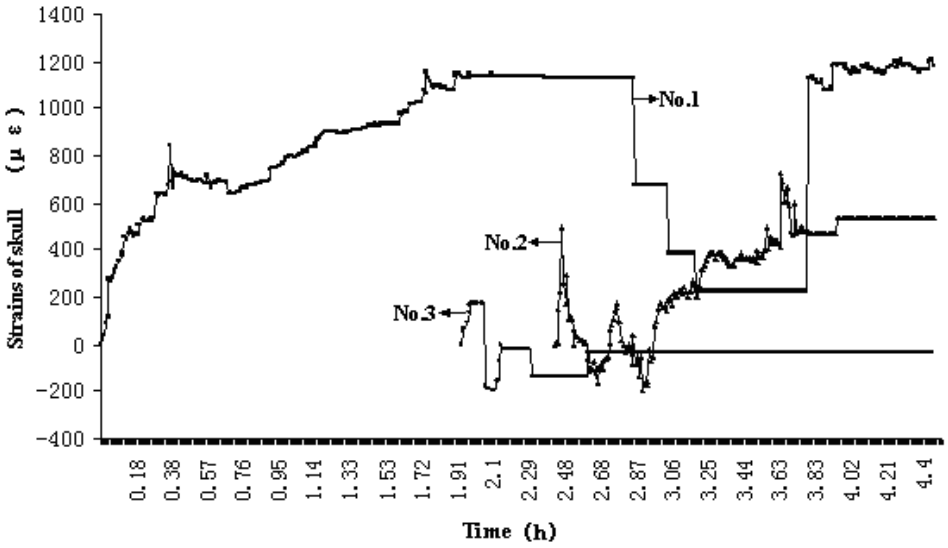

Figure 6. Strain changes of rats' skull bone with the changing ICP. **No.1 rat**: The strain change was totally corresponding to the symptom. After placed strain foils on the exterior surface of skull bone and searched the internal carotid artery for about 1.9 h, strains became stable. A silicone rubber cylinder attached to a nylon surgical thread was inserted through the internal carotid artery in rats and the blood vessel was obstructed for about half an hour from 2.82 h. The strains of skull bone were reduced with the decreasing ICP during the period of cerebral ischemia from 2.82 to 3.3 h. The thread was suddenly pulled out of the carotid artery while 3.3 h or so. After the autoregulation and recirculation of blood in carotid artery for about 40 min, the strains went up and reached the stability after nearly 3.83 h. **No.2 rat**: The wound in carotid artery bled twice when the time was about 2.5 and 2.8 h. Then ICP was decreased for the hemorrhage from the carotid artery. Correspondingly, the strains curve appeared to be twice-sharp declines at 2.5 and 2.8 h respectively, and reached the stable state at 3.9 h or so. **No.3 rat**: The position to place strain foil wasn't level on the exterior surface of skull bone and damp-proof measures were hardly taken for the strain foil. The strain foil wasn't firmly placed on the skull, so the strains couldn't reflect the ICP change.

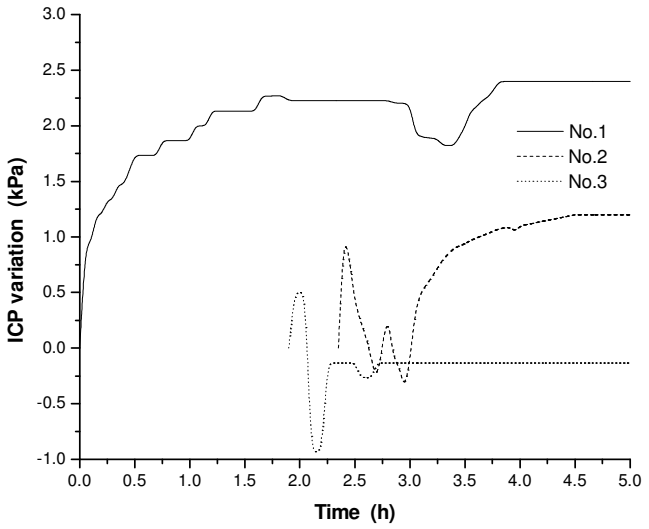

Figure 7. ICP changes of three rats with the measurable times. **No.1 rat**: ICP curve reached a plateau after about 1.9 h and was decreased during the period of cerebral ischemia from 2.82 to 3.3 h. Since the thread was pulled out of the carotid artery while 3.3 h or so, ICP went up and reached the stable state after nearly 3.83 h. **No.2 rat**: ICP was twice decreased at 2.5 and 2.8 h respectively. ICP reached the stable state after the autoregulation at 3.9 h or so. The ICP change of **No.3 rat** was irregular.

up through the internal carotid artery. The strain changes of rats' skull bone are shown in Figure 6 with the changing ICP. According to the literature (Gefen et al., 2003), the average elastic modulus and Poisson's ratio of rats' parietal skulls are respectively 6.3 MPa and 0.499. The relationship between stress and strain is $\sigma = \varepsilon E$, here σ is stress, ε is strain, E is the elastic modulus. Based on the strain-electrometric mechanism and after the automatic conversion of strain gauge, ICP variation of rats' could be obtained by the strains of skull bone with the measuring times (Figure 7). The skull strains were consistent with ICP change. All recordings were completed within 4 h. No attempt was made for prolonged recordings.

DISCUSSION

The deformation scope of human skull was theoretically from 0.9 to 3.4 $\mu\varepsilon$ as the ICP changing from 1.5 to 5.0 kPa. In No.1 rat, the ICP responded immediately the strains of skull bone. The records of No.1 and No.2 rats showed the exact same variations and patterns. Similar recordings of ICP tendency for No.1 and No.2 rats were observed after the experiment. In No.1 and No.2 rats, the skull strains responded immediately after arterial punture and ascended sharply. In a few seconds after pulling the thread out of the carotid artery, ICP reached the valley pressure and then increased rapidlly. ICP variation showed a similar pattern with skull strains. Among all of the recordings, lower peak values from No.2 rat were observed, which were about 40 - 50% lower than the values from No.1 rat. We have noticed some leaking of blood from the wound in carotid artery, which might contribute to the ICP reduction. Finally, the recording of stable ICP was raised due to the obstruction. The curve of No.3 rat indicated that it was important to paste firmly strain foil on the skull bone, or else the strain couldn't reflect the ICP change.

Conclusion

According to the mechanism of mechanical deformation, the cranium can move and human skull - dura mater system is deformed as the ICP fluctuates. The timing of ICP to reach the peak value, and the slope of curve to decay to the plateau is almost identical between the skull strains and the ICP change.

REFERENCES

Brint S, Jacewicz M, Kiessling M, Tanabe J, Pulsinelli W (1988). Focal brain ischemia in the rat: methods for reproducible neurocortical infarction using tandem occlusion of the distal middle cerebral and ipsilateral common carotid arteries. J. Cereb Blood Flow Metab. 8: 474-485.

Charalambopoulos A, Fotiadis DI, Massalas CV (1998). Free vibrations of the viscoelastic human skull. International J. Eng. Sci. 36 (5-6): 565-576.

Gefen A, Gefen N, Zhu QL, Raghupathi R, Margulies SS (2003). Age-dependent changes in material properties of the brain and braincase of the rat. J. Neurotrauma 20: 1163-1177.

Jallo J, Saetzler R, Mishke C, Young WF, Vasthare U, Tuma RF (1997). A chronic model to simultaneously measure intracranial pressure, cerebral blood flow, and study the pial microvasculature. J Neurosci Methods 75: 155-160.

Kellie G (1824). An account of the appearances observed in the dissection of two of the three individuals presumed to have perished in the storm of the 3rd, and whose bodies were discovered in the vicinity of Leith on the morning of the 4th November 1821 with some reflections on the pathology of the brain. Edinburgh: Trans. Med. Chir. Sci. 1: 84-169.

Kusaka G, Calvert JW, Smelley C, Nanda A, Zhang JH (2004). New lumbar method for monitoring cerebrospinal fluid pressure in rats. J. Neurosci. Methods 135: 121-127.

Lundberg N (1960). Continuous recording and control of ventricular fluid pressure in neurosurgical practice. Acta. Psychiat. Neurol. Scand. (Suppl). 36: 149.

Miller JD, Pattisapu J, Peeler DF, Parent AD (1984). Intracranial pressure monitoring by flaccid-cuff catheter in an animal model. J. Physiol. 246: 533-541.

Monro A (1823). Observations on the structure and function of the nervous system. Edinburgh, Creech & Johnson, p. 5.

Noort van R, Black MM, Martin TR (1981). A study of the uniaxial mechanical properties of human dura mater preserved in glycerol. Biomaterials 2: 41-45.

Odgaard A (1997). Three-dimensional methods for quantification of cancellous bone architecture. Bone 20: 315-328.

Piekarshi K (1973). Analysis of bone as a composite material. Int. J. Eng. Sci. 11: 557-565.

Retzlaff EW, Jones L, Mitchell Jr FL, Upledger J (1973). Possible autonomic innervation of cranial sutures of primates and other animals. Brain Res. 58: 470-477.

Sutherland WG (1939). The cranial bowl, Mankato, Minn: Free Press Company.